Accepted for publication in ApJ

A candidate of a type-2 QSO at $z = 0.9$: Large X-ray absorption with a strong broad-Hα emission line [1]

Masayuki Akiyama

Subaru Telescope, National Astronomical Observatory of Japan, Hilo, HI, 96720

akiyama@subaru.naoj.org

Yoshihiro Ueda

Institute of Space and Astronautical Science, Sagamihara, Kanagawa, 229-8510, Japan

ueda@astro.isas.ac.jp

and

Kouji Ohta

Department of Astronomy, Kyoto University, Kyoto, 606-8502, Japan

ohta@kusastro.kyoto-u.ac.jp

ABSTRACT

Deep hard X-ray and near infrared observations of a type-2 radio-quiet QSO candidate at $z = 0.9$, AX J08494+4454, are reported. The 0.5–10 keV *Chandra X-ray Observatory* spectrum of AX J08494+4454 is hard, and is explained well with a power-law continuum absorbed by a hydrogen column density of $(2.3 \pm 1.1) \times 10^{23}$ cm^{-2}. The 2–10 keV luminosity of the object is estimated to be $7.2^{+3.6}_{-2.0} \times 10^{44}$ erg s^{-1}, after correcting the absorption, and reaches hard X-ray luminosities of QSOs. The large X-ray absorption and the large intrinsic luminosity support the original identification of AX J08494+4454 as a type-2 radio-quiet QSO. Nevertheless, the deep Subaru/IRCS J-band spectroscopic observation suggests the presence of a strong broad Hα emission line from AX J08494+4454. If

[1]Based on data collected at Subaru Telescope, which is operated by the National Astronomical Observatory of Japan, and University of Hawaii 2.2m Telescope, HI.

real, the broad Hα emission line has a velocity width of 9400 ± 1000 km s^{-1}, which corresponds to a typical broad-Balmer line velocity width of a luminous QSO. The existence of the strong broad Hα line means that the object is not a type-2 QSO, but a luminous cousin of a Seyfert 1.9 galaxy in the source-frame optical spectrum. The Balmer decrement of broad lines, and the broad Hα emission to the hard X-ray luminosity ratio suggest that the nucleus is affected by dust extinction with A_V of $1 - 3$ mag in the optical wavelength. Optical colors and faint optical magnitudes of AX J08494+4454 are consistent with the model. The estimated amount of dust extinction is much smaller than that expected from the X-ray column density ($A_V = 130 \pm 60$ mag).

Subject headings: galaxies:active — galaxies:individual(AX J08494+4454) — infrared:galaxies — quasars:general

1. Introduction

"Type-2 QSO" is a missing population of AGNs which are radio-quiet narrow-line QSOs, i.e., luminous cousins of Seyfert 2 galaxies, or radio-quiet analogues of high-redshift radio galaxies. So-called unified scheme of Seyfert galaxies explains differences between Seyfert 1 and 2 galaxies with a difference of viewing angle to a nucleus surrounded by a dusty torus system (Antonucci 1993). QSOs are thought to be luminous versions of Seyfert galaxies. If the unified scheme holds for QSOs, then they should have a similar nucleus and dusty torus system in their center. Seyfert 2 galaxies outnumber Seyfert 1 galaxies in the local universe (Huchra and Burg 1992), and if that ratio can be extrapolated to higher luminosities, then we should expect many type-2 QSOs to be detectable in the high-redshift universe. Strikingly, none have been convincingly detected to date. The existence of absorbed high luminosity AGN has been postulated to account for the hard X-ray spectrum of the cosmic X-ray background; there should be three times more absorbed narrow-line QSOs than non-absorbed broad-line QSOs (Comastri et al. 1995).

Recently, deep hard X-ray surveys with imaging satellites detect several candidates of type-2 QSOs in the high-redshift universe (Almaini et al. (1995); Ohta et al. (1996), hereafter Paper I; Norman et al. (2001); Dawson et al. (2001)). These objects have hard X-ray luminosities as luminous as broad-line QSOs, and their hard X-ray spectra suggest that their X-ray nuclei are obscured. In the observed optical wavelength, they do not show the broad components in permitted emission lines, like Seyfert 2 galaxies. But this evidence is insufficient to definitely identify these objects as luminous versions of Seyfert 2 galaxies, because the characteristic point of Seyfert 2 galaxies is that no broad Hα emission line (above

a certain level). Therefore, in order to discuss similarities to Seyfert 2 galaxies, we need to cover source-frame Hα emission line. It should be noted that majority of AGNs in the local universe meets this criterion (Maiolino and Rieke 1995). Actually, for the candidate of type-2 QSO found by Almaini et al. (1995), later observation in the near-infrared wavelength revealed the presence of a strong broad Hα emission line and the object was reassigned as a type-1.9 QSO (Georgantopoulos et al. 1999). So far there is no hard-X-ray-selected type-2 QSO which is confirmed to follow the strict definition of Seyfert 2 (see also Halpern et al. (1999)). If there is no true type-2 QSO in the universe, it is suggested that QSOs are not simple luminous extension of Seyfert galaxies.

AX J08494+4454 is another candidate of a type-2 QSO at $z = 0.9$. It was found in the course of the optical identification of *ASCA* deep survey in Lynx field (Paper I). Based on the large hard X-ray luminosity, hard X-ray spectrum, which reflects a heavy absorption to the nucleus, and absence of broad Hβ emission line, the object is identified as a type-2 QSO (Paper I). Later J-band spectroscopic observation targeted on the redshifted Hα emission line does not show the presence of a strong broad Hα emission line at all (Nakanishi, et al. (2000), hereafter Paper II).

In this paper, results of a deep hard X-ray observation with *Chandra X-ray Observatory* and a deeper near-infrared observation of a redshifted Hα emission line with Subaru telescope of AX J08494+4454 are reported. The X-ray spectrum of the object establishes the large absorption column density along the line of sight to the nucleus. Although the previous near-infrared spectroscopy of AX J08494+4454 did not detect a significant broad Hα emission line, the deeper near-infrared spectrum reveals the probable existence of a very broad Hα emission line, whose strength suggests the broad-line is not affected severely by dust absorption. We discuss the discrepancy between source-frame optical and X-ray absorption and no existence of "type-2 QSOs". Throughout this paper, we use $q_0 = 0.5$ and $H_0 = 50$ km s^{-1} Mpc^{-1}.

2. Observations and Results

2.1. X-ray Observation with *Chandra*

2.1.1. Observation

AX J08494+4454 was observed with the *Chandra X-ray Observatory* in the 0.5–10 keV band on 2000 May 3 (ObsID=1708) and May 4 through 6 (ObsID=927) in the course of deep observations of the Lynx field (object name = CL 0848.6+4453). AX J08494+4454 was located in the ACIS-I3 chip at the row number of about 800. To mitigate the effect of

degradation by the Charge Transfer Inefficiency (CTI), we applied an improved technique developed by Townsley et al. (2000) for the the level 1 event data. This improved the spectral resolution to 4.4% (FWHM) at 3.4 keV (corresponding to 6.4 keV at $z = 0.8858$). Then the data were analyzed in a standard way using the CIAO 2.1 software. We used only events of *ASCA* grade 0, 2, 3, 4, and 6. After excluding periods of the background flares, we obtained a net exposure of 45 ksec for the May 3 observation and 119 ksec for the May 4–6 observation.

We detected AX J08494+4454 in the ACIS images as a point-like source from the both data sets. The position determined by *Chandra* is $\alpha = 8^{\rm h}49^{\rm m}27^{\rm s}.77$, $\delta = +44^\circ54'57''.6$ (J2000), after correcting the aspect solution according to the method available at the *Chandra* Science Center web page. The position error was conservatively estimated to be 1 arcsec: we confirmed the accuracy by cross correlating the position of a Tyco-catalog star and other APM catalog sources located in the field of view of the ACIS-I arrays. The X-ray source position is $0''.5$ east and $0''.6$ south of the optical position, and the X-ray and optical positions agree with each other within the uncertainty. The accurate X-ray position clearly rejects the possibility that the X-ray emission comes from a no-emission-line object $2''$ west (see Paper I and II).

2.1.2. Spectral Analysis

For an extraction of the spectrum, we accumulated events around the source position within a radius of 5 arcsec. The background spectrum was taken from a nearby, bright-source free region in the same chip. The background count rate was only 1% to the source photons in the 0.5–10 keV band and was not important. Examining the light curve and spectrum, we found that both the flux level and spectral shape of AX J08494+4454 were constant throughout the two observations within the statistical error. We thus summed the spectra of the two data sets with a total exposure of 164 ksec to obtain the best photon statistics. For a spectral fit, we used an appropriate response matrix file in which the above CTI correction is taken into account. Considering possible calibration uncertainties at low energies, we added a systematic error of 20% to each spectral bin below 1.2 keV. Spectral analysis was performed using the XSPEC package.

Figure 1 shows the *Chandra* ACIS spectrum of AX J08494+4454 folded with the detector response. As recognized from the figure, the X-ray spectrum is hard; the observed flux was 7×10^{-15} ergs cm^{-2} s^{-1} (0.5–2 keV) and 1.3×10^{-13} ergs cm^{-2} s^{-1} (2–10 keV), which are consistent with the previous *ASCA* observation (Paper I). In the spectral fit performed below, we assume Galactic absorption with a hydrogen column density fixed at $2.6{\times}10^{20}$ cm $^{-2}$, as estimated from HI observations by Dickey & Lockman (1990).

First we fit the spectrum with a single power law continuum with an intrinsic absorption at source frame. As a result, we obtained a photon index of 1.2±0.2 and a hydrogen column density of $(7 \pm 1) \times 10^{22}$ cm^{-2}. The fit was not acceptable ($\chi^2 = 79$ for the degree of freedom of 56), however, leaving a soft excess below $\simeq 1.2$ keV. Although we have to bear in mind possible calibration uncertainties in the current response matrices, we could attribute this to the presence of a scattered and/or less absorbed component (i.e., partial covering model). Such components have been observed in many of nearby Seyfert 2 galaxies (e.g., Turner et al. (1997)). Accordingly, we fit the spectrum with two absorbed power laws with different absorptions and normalizations, represented by the formula $AE^{-\Gamma}[f\,e^{-N_{\rm H1}\sigma(E)}+(1-f)\,e^{-N_{\rm H2}\sigma(E)}]$, where E is the source-frame photon energy in keV, Γ is the photon index, A is the normalization at 1 keV, $\sigma(E)$ is the photo-electric absorption cross section (Morisson & McCammon 1983), $N_{\rm H1}$ and $N_{\rm H2}$ are hydrogen column densities, and f represents the covering fraction. We find that the model can reproduce the observed continuum well. The best fit parameters are given in Table 1; the hydrogen column density is $N_{\rm H1} = (2.3 \pm 1.1) \times 10^{23}$ cm^{-2} and the absorption corrected source-frame 2–10 keV luminosity goes up to $7.2^{+3.6}_{-2.0} \times 10^{44}$ erg s^{-1} with an intrinsic photon index of 1.93 ± 0.44.

Finally, we add an iron K emission line at the source frame, which is expected as a result of reprocessing from the X-ray absorbing matter. We here consider only a narrow line and assume a 1σ intrinsic width of 0.02 keV: this corresponds to the velocity width of ∼900 km s^{-1}, which is chosen to be comparable to the widths of optical emission lines (600 km s^{-1}; Paper I). We obtain the center energy to be 6.51±0.14 keV with an equivalent width of 148^{+150}_{-142} eV at the source frame (Table 1). The center energy indicates that it originates from cold (or warm) ambient matter. The maximum allowed value for the equivalent width of the iron K line, ≃300 eV, rules out that the observed spectrum consists purely of a scattered or reflected component, which would produce an equivalent width of 1–3 keV (e.g., Matt, Brandt, and Fabian 1996). This gives strong evidence that a significant fraction of the observed emission comes directly from the central source. We plot the best fit model of each component in Figure 1 with residuals in the lower panel.

The relation between the obtained source-frame equivalent width of iron-K line and the absorption column density is consistent with the presence of surrounding matter around the central source in a spherical or torus-like geometry. For example, in the simplest case that a spherical gas with a uniform density surrounds the central source, we expect an equivalent width of about 100–300 eV for a column density of $N_{\rm H} = (1-3)\times10^{23}$ cm^{-2} assuming a power law spectrum with $\Gamma = 1.7$ (e.g., Inoue (1985); Leahy and Crighton (1993)). For a typical obscuring torus model as defined by Ghisellini, Haardt and Matt (1994) in their Figure 1, an iron-K emission is produced with an equivalent width of 40–110 eV for $N_{\rm H} = (1-3) \times 10^{23}$ cm^{-2} when we view through the torus having an opening angle $\theta = 30^\circ$ (see their Figure 3).

The source-frame equivalent width of 148^{+150}_{-142} eV is explained by this torus model having the same column densities as in the line of sight.

2.2. *J*-band Spectroscopic Observations with IRCS/Subaru

2.2.1. Observation and Data Reduction

J-band spectroscopic observations of AX J08494+4454 were done with InfraRed Camera and Spectrograph (IRCS; Kobayashi et al. (2000)) attached to Subaru telescope on 21 March 2001. A *J*-band grism, which covers a wavelength region from 1.18μm to 1.38μm with the fifth order, and a reflective slit with 0.″6 width were used. In the configuration, the spectral resolution (R) was 343 and the dispersion was 3.7 Å pixel^{-1}. The spatial scale was 0.″058 pixel^{-1}, which is over-sampling under the 0.″35 seeing condition during the observations. Because the seeing size was smaller than the slit width, the higher spectral resolution than R of 343 was achieved for the object. The spectra were taken at 2 positions, hereafter A and B positions, of the slit which separate 7″ apart. One set of a dithering pattern consists of four spectra taken at A, B, B, and A positions. At each position 120 s integration was made and 5 dithering sets were taken. Thus, the total effective integration time was 2400 s. The observation was done at the object airmass from 1.1 to 1.2. Before the observation, a field A0 type star (SAO42433, $V = 6.6$ mag) was also observed at an airmass of 1.2 for the atmospheric absorption correction.

The data were reduced in the following manner; at first from each set of A and B positions or B and A positions combinations, the B position image was subtracted from the A position image. Most of night sky emission lines were removed with the process, but for the strongest night sky lines, they could not be removed completely, thus we removed the remaining night sky emissions, using the sky spectra along the slit direction. After that all A minus B images were flat fielded with a flat image which was made from subtracting images taken with a slit-illumination lamp (halogen lamp) off from images with the lamp on. Next, all the flat-fielded images were stacked and the wavelength calibration of the stacked image was done using night sky lines in the raw object frame. The uncertainty of the wavelength calibration was 10 Å (r.m.s.). After optimum extraction method was applied to extract one dimensional spectral data from the two dimensional stacked image, spectra taken at A position and B position were summed. Atmospheric absorption and a sensitivity function were corrected using spectra of the standard star which were reduced in the same manner. Flux calibration was done based on the *J*-band magnitude of the object as described below.

During the telescope acquisition of *J*-band spectroscopic observation, four images with a

45 s integration time each were also taken with the J-band filter of Mauna Kea Observatory Near-Infrared filter set. For the flux calibration, three photometric standard stars were observed (UKIRT Faint Standard stars; FS021[J=12.976mag], FS125[J=10.789mag], and FS127[J=11.947mag]). Four images of AX J08494+4454 were taken at different position in the detector, thus at first we subtracted each image from another image in order to subtract sky background. After that these sky subtracted images were flat-fielded with a flat image which was made from subtracting images taken with the field-illumination lamp (halogen lamp) off from images with the lamp on. In each flat-fielded image, the signal to noise ratio of the object is high, thus we measured the count rate in each image, independently. The measured count rates were consistent within 6 %. The standard star frames were reduced in the same manner. Count rates of each star taken at different positions of the detector were consistent within 2 %. Based on the scatter of calculated count rate to magnitude conversion factor for the 3 standard stars, the uncertainty of the flux calibration was estimated to be 0.05 mag. The measured J-band magnitude of AX J08494+4454 is 17.79 ± 0.08 mag, and the flux calibration of the J-band spectrum was done with the J-band magnitude. The size of the object in the J-band image was FWHM of 5.9 pixel ($0\farcs35$), which is the same as those of other stellar objects. No extended component was detected. Because the slit width was wider than the object size, all parts of the object should be sampled.

2.2.2. Results

The J-band spectrum of the object is shown in Figure 2. A strong narrow Hα emission line is detected, and it shows a shoulder in the red side, which comes from [N II]λ6583 emission line. A continuum emission of the object is also detected. There is a weak bump at the wavelength corresponding to [S II]$\lambda\lambda$6718,6733 emission lines. It should be noted that the [S II]$\lambda\lambda$6718,6733 region suffers from a strong night sky emission line. The narrow-Hα line strength and the continuum flux level are consistent with those obtained in the previous J-band spectrum of AX J08494+4454 (Paper II). Although in the previous spectrum no significant broad-Hα emission line was detected, in the continuum emission of the new J-band spectrum there is a bump in the wavelength range from 12000Å to 13000Å, and an existence of a broad Hα emission line is suggested. Because of a low efficiency of the grism in the wavelength range below 12300 Å, the signal to noise ratio in the wavelength range was low, and the blue part of the broad component is uncertain. The broad component could be an artifact of an error of the sensitivity correction. In order to examine whether the broad Hα emission line is due to an error of the sensitivity correction, we apply the sensitivity function which is used to the spectrum of AX J08494+4454 to a spectrum of a bright G5V type star taken in the next night of the observation of AX J08494+4454. The

corrected spectrum of the star is consistent with the model spectrum of a G5V type star (Kurucz 1979) within 10% in the wavelength range above 12000Å, and we expect that the broad Hα feature is not due to an error of the sensitivity correction. It should be noted that the probable broad emission line has a much larger velocity width ($\sim$ 9000 km s^{-1}) than that assumed in Figure 1 of Paper II (3000 km s^{-1}).

In order to determine the strength and the velocity width of these narrow and broad emission lines, fitting to the obtained spectrum with the χ^2 minimization method is applied in the wavelength range from 12300Å to 13500Å. In the fitting, we assume that all the redshifts for the narrow-Hα, broad-Hα, narrow-[N II]$\lambda\lambda$6548,6583, and narrow-[S II]$\lambda\lambda$6718,6733 emissions are the same, and the velocity widths of the narrow-emission lines are also the same. The flux ratio between [N II]λ6548 and [N II]λ6583 is fixed. The best-fit wavelengths, fluxes, and velocity widths of each emission lines are summarized in Table 2 and the result of the fitting is shown in Figures 1b and 1c. One sigma uncertainties of each free parameters are listed also. All of the uncertainties of emission line fluxes are dominated by J-band photometry uncertainty, except for the flux of [S II]$\lambda\lambda$6718,6733 emission lines.

The resulting redshift of the narrow-Hα emission line is 0.8866 ± 0.0008, which agrees with that obtained in the optical spectrum ($z = 0.8858 \pm 0.0002$; PaperI) and obtained in the previous J-band spectrum ($z = 0.8857 \pm 0.0002$; Paper II). The spectral resolution measured with night sky emission lines in the frame is FWHM of 30Å, which corresponds to 8 pixel and $0\farcs47$ in the spatial direction. Resolution for the object emission line should be higher than that of the night sky lines because the FWHM of the object ($0\farcs35$) is smaller than the slit width in the spatial direction. Considering the FWHM difference between the object and the slit images, we estimated the resolution for the object to be 22 Å, which corresponds to 533 km s^{-1}. Using this value as instrumental broadening, we estimated intrinsic velocity widths of narrow- and broad-emission lines to be FWHM of 590 ± 60 and 9400 ± 1000 km s^{-1}, respectively.

The probable existence of the strong broad Hα emission line and non-detection of a broad Hβ emission line suggest AX J08494+4454 is similar to Seyfert 1.9 galaxies. However, the width of the broad Balmer emission line corresponds to the smallest value of high-luminosity radio-quiet QSOs ($M_V < -28$ mag), and is the largest value of low-luminosity radio-quiet QSOs ($M_V > -25$ mag) (McIntosh et al. 1999). Interpolating the two samples of radio-quiet QSOs, we expect that the velocity width of AX J08494+4454 is consistent with QSOs with M_V of about -26 mag. Therefore, the large velocity width of the broad-line of AX J08494+4454 suggests that the object has a high-luminosity QSO nucleus in its center.

The narrow-line width is consistent with that of narrow-[O III]λ5007 emission line in the optical wavelength (600 km s^{-1}; Paper I) and that of typical values of narrow-line region

of Seyfert galaxies (Whittle 1992). The [N II]λ6583 to narrow-Hα flux ratio corresponds to the smallest value among Seyfert 2 galaxies (Veilleux and Osterbrock 1987). The large [O III]λ5007 to narrow-Hβ flux ratio (Paper I) distinguishes the object from HII region like objects.

2.3. Optical Photometric Observation and Results

Optical photometric observations in Mould B, V, R, and I bands were made with Tektronix 2048×2048 CCD camera at University of Hawaii (UH) 88″ telescope on 1999 March 5 and 6. Exposure times of the observations were 3600, 2100, 1800, and 1200 s in B, V, R, and I bands, respectively. During the observing run, 50 Landolt's standard stars (Landolt 1992) were observed. The seeing size was 1.″0 and the pixel scale was 0.″22 pixel^{-1}. The imaging data were analyzed with IRAF. Bias subtraction and flat-fielding with dome flats were performed. Based on the scatters of the count rate-to-magnitude conversion factors of the observed Landolt's standard stars, the uncertainties in the photometric calibrations were estimated to be 0.03, 0.06, 0.03, and 0.06 mag in B, V, R, and I bands, respectively. The B, V, R, and I band magnitudes were measured to be 22.14 ± 0.06, 21.40 ± 0.08, 20.87 ± 0.06, and 20.20 ± 0.08 mag, respectively. The uncertainty includes the flux calibration uncertainty as described above, uncertainty of flat-fielding in the object frame, and the sky subtractions. These results are summarized in Table 3. The I band magnitude is consistent with a previous measurement (20.3 ± 0.3; Paper II). The I band magnitude of the western object is 19.81 ± 0.08 mag and the summed magnitude of the eastern and the western objects is 19.24 mag. This is 1.1 mag brighter than that estimated from the optical spectrum (20.3 mag; Paper I). The discrepancy can be due to an underestimate of the object brightness in Paper I, because the slit might not have been centered on the object. In the B-, V-, and R-band images, AX J08494+4454 has slightly larger image size (FWHM of 5.1 pixel) than stellar objects in each frame (FWHM of 4.4 pixel). In the I-band, the image is elongated by a guiding error, no measurement on the image size was made.

3. Discussions: Discrepancy Between Optical and X-ray Absorption

The hard X-ray and narrow-emission line properties of AX J08494+4454 are consistent with those of Seyfert 2 galaxies. Its X-ray spectrum can be fit with an absorbed power law with a column density of $N_{\rm H} \simeq (2.3 \pm 1.1) \times 10^{23}$ cm^{-2} at the source frame. The results on the X-ray spectrum generally agree with the picture of the unified scheme for type-2 AGNs (Awaki et al. 1991), except that the intrinsic 2–10 keV luminosity ($7.2^{+3.6}_{-2.0} \times 10^{44}$

ergs s^{-1}) is larger than those of nearby Seyfert 2 galaxies. The hard X-ray to [O III]λ5007 luminosity ratio of the AX J08494+4454 follows the extension of those of Seyfert 1 and 2 galaxies (Halpern et al. (1998)).

The probable existence of the strong Hα broad-emission line conflicts with the large X-ray absorption, which corresponds to A_V of 130 ± 60 mag with Galactic extinction curve and gas-to-dust ratio. In order to quantitatively examine the discrepancy, we estimated the amount of dust absorption to the broad-line region with three indicators; Balmer decrements, hard X-ray to Hα luminosity ratio, and shape of optical continuum emission.

We can only put lower limit on the Balmer decrement of AX J08494+4454 because broad Hβ emission line was not detected in the optical spectrum (Paper I). The upper limit on the flux of the broad Hβ emission line with the velocity width of 9400 km s^{-1} is 1.8×10^{-15} erg s^{-1} cm^{-2}. Thus, the lower limit on the Balmer decrement to the broad-line region is 4.8, and we obtain the lower limit on the absorption to the nucleus as A_V of 1.2 mag, assuming that an intrinsic Balmer decrement is the typical value in broad-line QSOs (3.1; Brotherton et al. (2001)), and the nuclear absorption follows the Galactic extinction curve.

Based on the relation between hard X-ray and Hα luminosity, the luminosity of the broad Hα emission of object with hard X-ray luminosity of $7.2^{+3.6}_{-2.0} \times 10^{44}$ erg s^{-1} cm^{-2}, should be $(0.5 - 40) \times 10^{43}$ erg s^{-1} cm^{-2} (Ward et al. 1988). The measured Hα flux corresponds to Hα luminosity of $(3.9 \pm 0.5) \times 10^{43}$ erg s^{-1} cm^{-2}, which falls within the above range. The upper limit on the absorption to the Hα emission is estimated to be A_α of 2.7 mag, that is converted to A_V of 3.4 mag with the Galactic extinction curve.

The reddening to the nucleus is also estimated from the shape of optical and near infrared continuum emission, if the optical continuum is dominated by the reddened nuclear emission. AX J08494+4454 has a red $I - K$ color and, there are three possibilities to the origin of the red color: reddened nuclear continuum, old stellar population of host galaxy, and reddened young stellar population. In Figure 3, $B - V$, $V - I$, and $I - K$ colors of AX J08494+4454 are plotted together with colors of an average QSO spectrum (Brotherton et al. 2001), those with reddening of $A_V = 1$ mag, and colors of model galaxies. We do not use the R- and J-band magnitudes, because the wavelength ranges are affected by strong [O II]λ3727 and Hα emission lines, respectively. The average QSO colors have scatter of about 0.2 mag (r.m.s.) (Richards et al. 2001). For galaxy models, two galaxy color evolution models are plotted (Kodama, Arimoto 1997): 1) Elliptical model (plotted with a solid line) in which star formation occurs during the first 0.353 Gyr with an initial mass function with a slope of 1.20; after that the galaxy evolves passively. The model parameters well reproduce the reddest and brightest ($M_V = -23$ mag) class elliptical galaxy in the Coma cluster (Kodama et al. 1998). 2) Disk model (plotted with a dotted line) is used in which

star formation occurs constantly with the same initial-mass function as that in the elliptical model. The colors of these models at redshift of 0.9 with ages from 0.01 Gyr to 5 Gyr, which corresponds to the age of the universe at the redshift, are shown with tracks. The colors of the reddened ($A_V \sim 1$ mag) average QSO spectrum (filled triangles) are close to the observed colors of AX J08494+4454. While AX J08494+4454 does not have as red color as old elliptical model in $V-I$ color, which reflects the size of 4000Å break at the redshift of 0.9, thus an old stellar population can not be the origin of the optical continuum. Considering the direction of reddening vector, we can also reject the possibility that an absorbed young stellar population makes the red color of AX J08494+4454. Therefore, the reddened nuclear continuum is the most plausible origin of the red optical to near infrared colors. The J-band spectrum of AX J08494+4454 also supports the model, because the source frame equivalent width of the broad Hα line (380±50 Å) is similar to those of broad-line QSOs (300 ± 100 Å, Brotherton et al. (2001)), and contamination from stellar continuum emission should be negligible in the J-band. On the other hand, the optical images of AX J08494+4454 are slightly extended. From deconvolution of an I-band image of AX J08494+4454 the contribution of the host galaxy to the total light is estimated to be $45-55\%$ (Paper II). There are $0.2-0.3$ mag discrepancy between the colors of AX J08494+4454 and the $A_V \sim 1$ mag absorbed QSO model, and the colors of AX J08494+4454 are shifted to the tracks of the galaxy models. The discrepancy can be due to the contamination of the host galaxy component.

The overall spectral energy distribution (SED) of AX J08494+4454 is also consistent with a QSO SED affected with A_V of 1 mag in the optical wavelength. In Figure 4, the energy densities at 8 keV, 4 keV, B-, V-, I-, K-bands (Paper II) and 1.4 GHz (Oort 1987) are plotted with an average radio-quiet QSO SED taken from Elvis et al. (1994). In the hard X-ray range, we plotted the intrinsic power-law component determined by the X-ray spectral fitting. *IRAS* survey upper limits (Paper I) are also plotted with downward arrows. The average QSO SED is normalized to have the same energy density with AX J08494+4454 at 1.4 GHz. The faint optical magnitudes are explained well with average QSO spectrum affected by A_V of 1 mag in the optical wavelength (upper dashed line in Figure 4).

To summarize the optical extinction estimations, the extinction to the nucleus is estimated to be A_V of $1-3$ mag from the strength of broad Hα line, and the extinction is consistent with the optical colors and the overall SED of AX J08494+4454. The estimated amount of absorption is significantly smaller than that expected from the X-ray absorption. The estimated $A_V/N_{\rm H}$ value of AX J08494+4454 is $(0.3-2.5)\times10^{-23}$ mag cm^{-2}, and more than 20 times smaller than those measured in the Galaxy (e.g., Predehl and Schmitt (1995)). Similar discrepancy of values between absorption from broad Balmer (or Paschen)-line ratio and from X-ray spectrum is reported for objects with $N_{\rm H} \geq 10^{22}$ cm^{-2} and with

broad-Balmer and/or Paschen lines (e.g., Maiolino et al. (2001a)). In Seyfert 2 galaxies, the amount of absorption determined from L-band reddening is also much smaller than the expected absorption derived from the hard X-ray observation (Alonso-Herrero et al. (1997)). Similar discrepancy is reported even in the line of sight to the Galactic center (Maeda et al. (2001)). The discrepancy can be explained with a smaller dust to gas mass ratio which may due to dust sublimation in the X-ray absorbing matter, the size difference between optical and X-ray emitting region, or different dust size distribution in AGNs (Maiolino et al. (2001b)).

In hard-X-ray-selected heavily-absorbed AGNs, there may be a discrepancy of amount of dust reddening between Seyfert galaxies and QSOs. AX J08494+4454 has the hardest X-ray spectrum in the X-ray sources detected in the Lynx field with *Chandra*, and it is confirmed that the object is affected by the heavy X-ray absorption, but AX J08494+4454 probably has broad Hα emission as strong as normal QSOs. In contrast, very hard X-ray sources detected in wider area *ASCA* surveys are identified with low-redshift Seyfert 2 galaxies that do not show strong broad Hα emission line at all (Iwasawa et al. 1997; Akiyama et al. 1998). Their estimated amounts of X-ray absorption are similar to that of AX J08494+4454 but their Hα emission lines are much more affected by dust extinction than in AX J08494+4454. The discrepancy between the high-redshift QSO and the low-redshift Seyferts may suggest that X-ray luminous QSOs have different internal structure from low-luminosity Seyfert galaxies: on average, QSOs have smaller $A_V/N_{\rm H}$ value than low-luminous Seyfert galaxies, and QSOs are less affected by dust reddening.

We are grateful to members of UH88″ telescope, Subaru Telescope and IRCS team, especially, Drs. Hiroshi Terada, and Naoto Kobayashi, who gave us invaluable advices on the J-band observations. We acknowledge Dr. Leisa Townsley for her kind support on the CTI correction of the *Chandra* ACIS data and Dr. Yoshitomo Maeda for his critical advice on the analysis. We would like to thank the referee, Dr. Paul Green, for valuable comments on the work.

REFERENCES

Akiyama, M., et al. 1998, ApJ, 500 173

Almaini, O., Boyle, B. J., Griffiths, R. E., Shanks, T., Stewart, G. C., and Georgantopoulos, I. 1995, MNRAS, 277, 31

Alonso-Herrero, A., Ward, M.J., and Kotilainen, J.K. 1997, MNRAS, 288, 977

Antonucci, R.R.J. 1993, ARA&A, 31, 473

Awaki, H., Koyama, K., Inoue, H., and Halpern, J.P. 1991, PASJ, 43, 195.

Brotherton, M.S., Tran, H.D., Becker, R.H., Gregg, M. D., Laurent-Muehleisen, S.A., and White, R.L. 2001, ApJ, 546, 775

Comastri, A., Setti, G., Zamorani, G., and Hasinger, G. 1995, A&A, 296, 1

Dawson, S., Stern, D., Bunker, A.J., Spinrad, H., and Dey, A. 2001, ApJ, in press, astro-ph/0105043

Dickey, J.M., and Lockman, F.J. 1990, ARA&A, 28, 215

Elvis, M., et al. 1994, ApJS, 95, 1

Georgantopoulos, I., Almaini, O., Shanks, T., Stewart, G.C., Griffiths, R.E., Boyle, B.J., and Gunn, K.F. 1999, MNRAS, 305, 125

Ghisellini, G., Haardt, F., and Matt, G. 1994, MNRAS, 267, 743

Halpern, J.P., Eracleous, M., and Forster, K. 1998, ApJ, 501, 103

Halpern, J.P., Turner, T.J., and George, I.M. 1999, MNRAS, 307, L47

Huchra, J., and Burg, R. 1992, ApJ, 393, 90

Inoue, H., 1985, Space Science Reviews, 40, 317

Iwasawa, K., Fabian, A.C., Brandt, W.N., Crawford, C.S., and Almaini, O. 1997, MNRAS, 291, L17

Kobayashi N., et al. 2000, SPIE, 4008, 1056

Kodama, T., and Arimoto, N. 1997, A&A, 320, 41

Kodama, T., Arimoto, N., Barger, A.J., and Aragón-Salamanca, A. 1998, A&A, 334, 99

Kurucz, R.L. 1979, ApJS, 40, 1

Landolt, A.U. 1992, AJ, 104, 340

Leahy, D.A., and Crighton, J, 1993, MNRAS, 263, 314

Maeda, Y., et al. 2001, astro-ph/0102183

Maiolino, R., and Rieke, G.H. 1995, ApJ, 454, 95

Maiolino, R., et al. 2001a, A&A, 365, 28

Maiolino, R., Marconi, A., and Oliva, E. 2001b, A&A, 365, 37

Matt, G., Brandt, W.N., and Fabian, A.C. 1996, MNRAS, 280, 823

McIntosh, D.H., Rieke, M.J., Rix, H.-W., Foltz, C.B., and Weymann, R.J. 1999, ApJ, 514, 40

Morrison, R., and MnCammon, D. 1983, ApJ, 270, 119

Nakanishi, K., Akiyama, M., Ohta, K., and Yamada, T. 2000, ApJ, 534, 587 (Paper II)

Norman., C., et al. 2001, astro-ph/0103198

Ohta, K., Yamada, T., Nakanishi, K., Ogasaka, Y., Kii, T., and Hayashida, K. 1996, ApJ, 458, 57 (Paper I)

Oort, M.J.A. 1987, A&AS, 71, 221

Predehl, P., and Schmitt, J.H.M.M. 1995, A&A, 293, 889

Richards, G.T., et al. 2001, AJ, 121, 2308

Townsley, L.K., Broos, P.S., Garmire, G.P., and Nousek, J.A. 2000, ApJ, 534, L139

Turner, T.J., George, I.M., Nandra, K., and Mushotzky, R.F. 1997, ApJS, 113, 23

Veilleux, S., and Osterbrock, D.E. 1987, ApJS, 63, 295

Ward, M.J., Done, C., Fabian, A.C., Tennant, A.F., and Shafer, R.A. 1988, ApJ, 324, 767

Whittle, M. 1992, ApJ, 79, 49

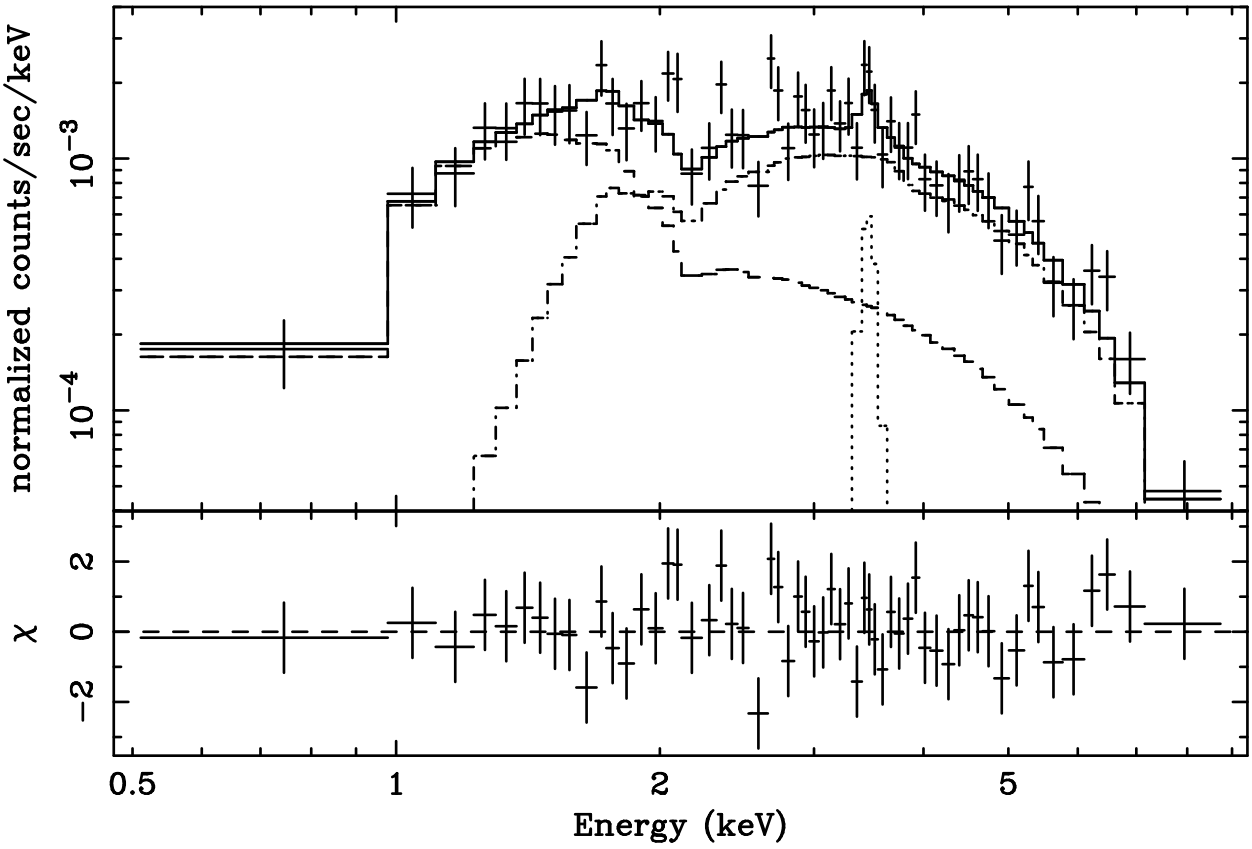

Fig. 1.— The *Chandra*-ACIS spectrum of AX J08494+4454. The best-fit model is plotted with solid line. The components of the model, the two power laws with different absorptions (dot-dashed and dashed lines) and an iron K emission line (dotted line), are also plotted.

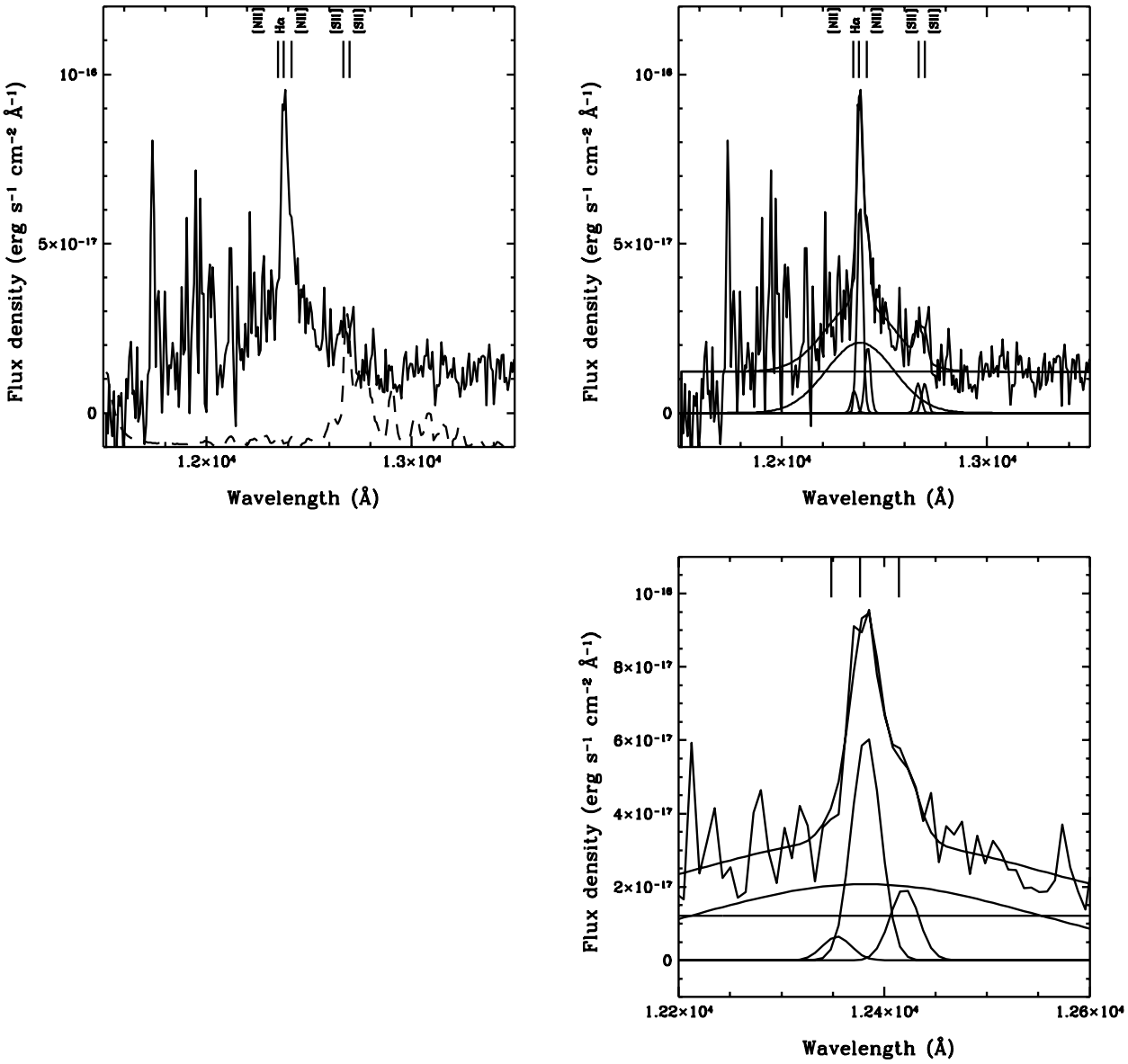

Fig. 2.— J-band spectrum of AX J08494+4454, a) (upper left) with a night sky spectrum in arbitrary unit (dashed line), and b) (upper right) with the best fit model spectrum. c) (lower right) same as b), but zoomed in the Hα, [N II]$\lambda\lambda$6548,6583 wavelength region. Identifications of emission lines are shown in each panel.

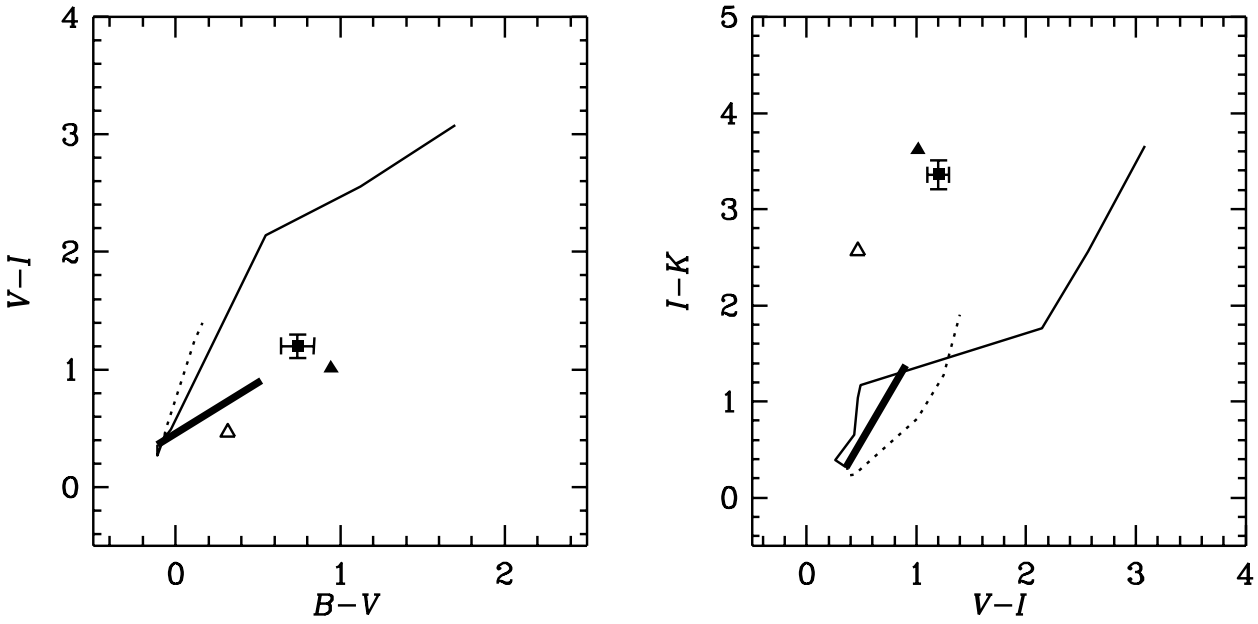

Fig. 3.— $B-V$ vs. $V-I$ (left) and $V-I$ vs. $I-K$ (right) diagrams for AX J08494+4454. Filled squares represent colors of AX J08494+4454. Open and filled triangles indicate colors of average QSO spectrum with no absorption and absorption with A_V of 1 mag. Thin solid and dashed lines represent colors of elliptical and disk galaxy models at redshift of 0.8858 with ages from 0.01 Gyr to 5 Gyr. Thick solid lines indicate effect of reddening on young stellar population model with an absorption of $A_V = 1$ mag.

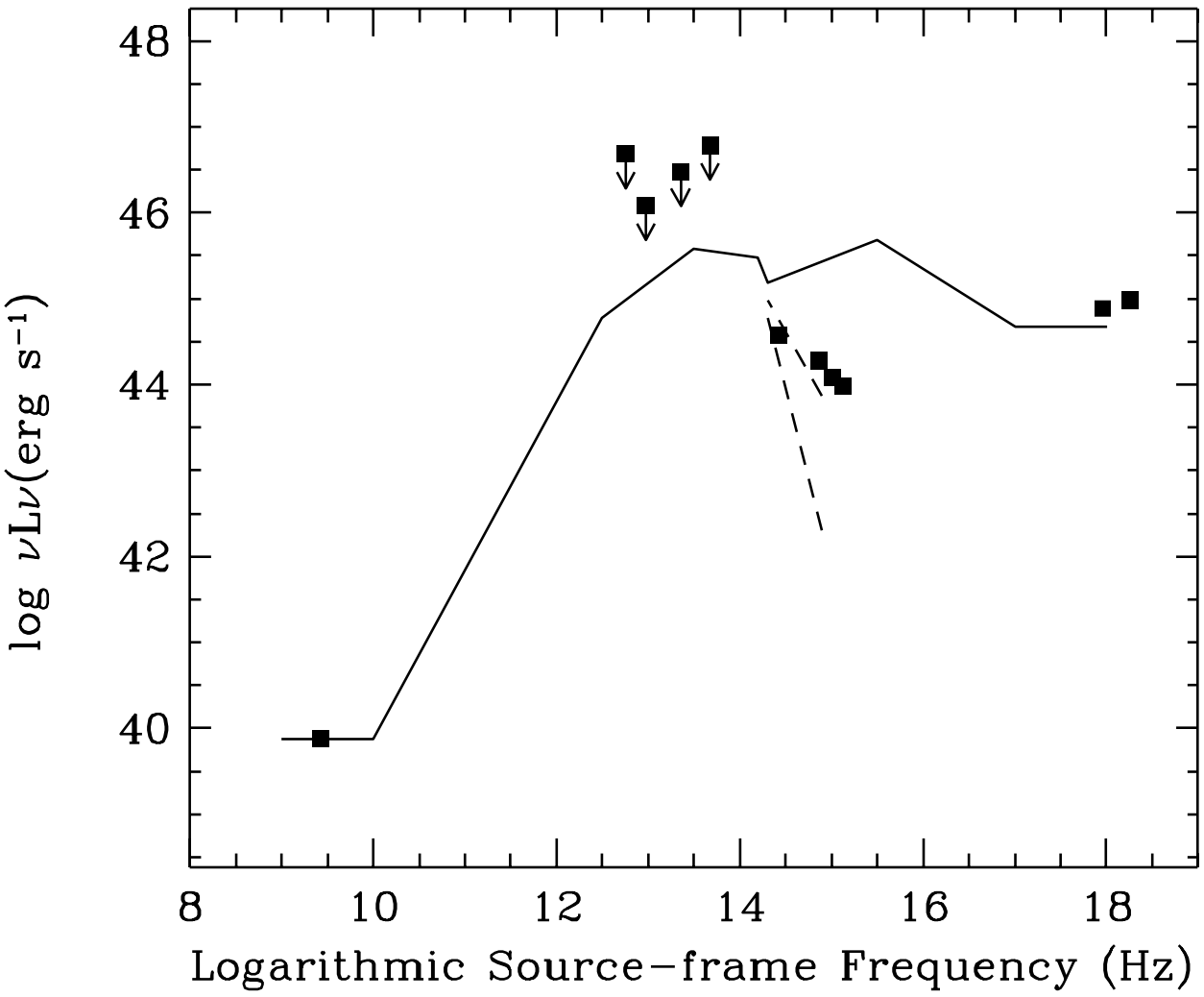

Fig. 4.— Spectral energy distribution (SED) of AX J08494+4454. Filled squares indicate data points of AX J08494+4454. Downward arrows represent *IRAS* upper limits for AX J08494+4454 (Paper I). Solid line indicates SED of an average radio-quiet QSO (Elvis et al. 1994) and is normalized at the data point observed at 1.4 GHz. Dashed lines represent optical SEDs affected by dust extinction with A_V of 1 mag (upper) and 2 mag (lower).

Table 1. Fitting Results of the *Chandra* Spectrum

A (10^{-5}cm^{-2} s^{-1} keV^{-1})	20^{+36}_{-13}
Γ	1.93±0.44
f	$0.84^{+0.08}_{-0.13}$
$N_{\rm H1}$ (10^{22} cm^{-2})	23±11
$N_{\rm H2}$ (10^{22} cm^{-2})	3.8±1.9
Luminosity[a](10^{44} erg s^{-1})	$7.2^{+3.6}_{-2.0}$
Line Energy (keV)	6.51±0.14
Equivalent Width[b](eV)	148^{+150}_{-142}
χ^2/dof	52.0/53

[a] The 2–10 keV luminosity of the power law component in the source frame corrected for absorption.

[b]Source frame.

Note. — The source-frame spectrum (at z=0.8858) is modeled by the formula $AE^{-\Gamma}[fe^{-N_{\rm H1}\sigma(E)}+(1-f)e^{-N_{\rm H2}\sigma(E)}]$, where E is the source-frame photon energy in keV, Γ is the photon index, A is the normalization at 1 keV, $\sigma(E)$ is the photo-electric absorption cross section (Morisson & McCammon 1983), f is the covering fraction, and $N_{\rm H1}$ and $N_{\rm H2}$ are hydrogen column densities. Spectral fit was performed assuming Galactic absorption of $N_{\rm H} = 2.6 \times 10^{20}$ cm^{-2}. Errors are 90% confidence limits for a single parameter.

Table 2. J band Emission Line Properties.

Name	Wavelength (Å)	Flux (erg s^{-1} cm^{-2})	Width (km s^{-1})	Luminosity (erg s^{-1})
[NII]6548	12354	2.3×10^{-16}	795	1.0×10^{42}
Broad-Hα	12382	$8.6 \pm 1.1 \times 10^{-15}$	9393 ± 1016, 9400[a]	3.9×10^{43}
Narrow-Hα	12382 ± 5	$2.2 \pm 0.3 \times 10^{-15}$	795 ± 61, 590[a]	9.9×10^{42}
[NII]6583	12419	$6.9 \pm 1.3 \times 10^{-16}$	795	3.1×10^{42}
[SII]6713	12664	$3.2 \pm 1.2 \times 10^{-16}$	795	1.4×10^{42}
[SII]6730	12697	$3.1 \pm 1.2 \times 10^{-16}$	795	1.4×10^{42}

Note. — All values with uncertainty are independent parameters in the fitting.

[a]After deconvolution of instrumental profile.

Table 3. Results of Optical Photometry.

B (mag)	V (mag)	R (mag)	I (mag)	J (mag)	K (mag)
22.14 ± 0.06	21.40 ± 0.08	20.87 ± 0.06	20.20 ± 0.08	17.79 ± 0.08	16.9 ± 0.1[a]

[a]Taken from Paper II.